lubricants

MDPI

Article

Capacitance Calculation of Cylindrical Roller Bearing—Modeling of the Cylinder Raceway and Cylinder Flange Contact

Jan Manteufel [1,*], Steffen Puchtler [2] and Eckhard Kirchner [1]

[1] Institute for Product Development and Machine Elements, Technical University of Darmstadt, Otto-Berndt-Str. 2, 64287 Darmstadt, Germany
[2] HCP Sense GmbH, Robert-Bosch-Straße 7, 64293 Darmstadt, Germany; puchtler@hcp-sense.com
* Correspondence: jan.manteufel@tu-darmstadt.de

Abstract

A precise understanding of the electrical properties of bearings is of great interest in many areas of application, especially in the context of electrification. The understanding of electrical properties allows for damage detection and sensory utilization of bearings. Previous research into the capacitive properties of rolling bearings has been limited to ball bearings. Cylindrical roller bearings, which are predominantly used in applications with large radial loads, have not been investigated so far. This paper develops a method to calculate the capacitance of cylindrical roller bearings. The calculation of the raceway–surface contact capacitance is adapted from ball bearings. In addition, a calculation method for the electrical capacitance in the flange contact is derived. Both calculation methods account for the geometric and operating conditions of the bearing and do not include any correction factors. To validate the calculation model, the capacitance of NU-208 and NJ-208 cylindrical roller bearings is measured and compared with the model results.

Keywords: cylindrical roller bearing; electrical capacitance; flange-contact; raceway contact; elastohydrodynamic lubrication

1. Introduction

In the automotive industry, there is an increasing trend of using electric motors driven by frequency converters instead of traditional combustion engines. However, these converters can induce harmful currents in adjacent components, such as bearings [1,2]. One of the most significant challenges in the development of electric vehicles is the prevention and prediction of current damage in bearings [3,4]. In order to proceed with this matter, it is necessary to thoroughly characterize and investigate the chains of effects in the bearing. In previous work, models for ball bearings have already been investigated [5–7].

In addition, capacitance measurement is used to determine the lubricating film thickness between two contact partners and validate models for calculating the lubricating film thickness [8–12]. To effectively establish a relationship between the lubricating film thickness and the capacitance, precise electrical models are required to reduce uncertainties.

Schirra et al. proved the possibility of using the electrical properties of bearing sensors to determine the effective load in bearings. They found that the primary factors influencing the electrical properties are the lubricating film thickness and the load distribution within the bearing [13].

Check for updates

Received: 5 March 2026
Revised: 2 April 2026
Accepted: 7 April 2026
Published: 9 April 2026

Copyright: © 2026 by the authors. Licensee MDPI, Basel, Switzerland. This article is an open access article distributed under the terms and conditions of the Creative Commons Attribution (CC BY) license.

This work presents a model for calculating the electrical capacitance of cylindrical roller bearings, considering the operational conditions and the geometry of the bearing. The model can be applied to both axially loaded and unloaded cylindrical roller bearings and is based on physical relationships to work without correction factors.

1.1. Roller Bearing Capacitance

When a bearing rotates with sufficient speed and lubricant, a separating lubricating film is formed at the rolling element contacts. With the separating lubricating film acting as a dielectric, the resulting electrical behavior of the bearing is capacitive. The capacitance can sufficiently be described by the equation for a plate capacitor in divisions and integral form, as shown in Equation (1). The determining variables are the relative permittivity of the dielectric ε_r, the permittivity of the vacuum ε_0, the distance between the two charge carriers h or $h(x,y)$, and the area A or $\mathrm{d}A$.

$$\begin{aligned} C &= \varepsilon_0 \cdot \varepsilon_\mathrm{r} \cdot \frac{A}{h} \\ C(x,y) &= \varepsilon_0 \cdot \varepsilon_\mathrm{r} \cdot \iint_A \frac{1}{h(x,y)} \,\mathrm{d}A \end{aligned} \tag{1}$$

The central lubricant film thickness h_0 is used as the distance between the charge carriers in the Hertzian area. This is calculated for line contact according to Equation (3) and for point contact according to Equation (2) [14,15]. The thickness of the lubricating film depends on the dimensionless radius R, the dimensionless velocity U, the dimensionless load W, the dimensionless material parameter G, and the semi-axis ratio k [14].

$$h_{0,\mathrm{point}} = R \cdot 2.69 \cdot U^{0.68} \cdot G^{0.49} \cdot W^{-0.073} \left(1 - e^{-0.68 \cdot \mathrm{k}}\right) \tag{2}$$

$$h_{0,\mathrm{line}} = R \cdot 3.06 \cdot U^{0.69} \cdot G^{0.56} \cdot W^{-0.1} \tag{3}$$

However, when a bearing is subjected to radial or axial loads, a load zone forms where the load is transferred. The capacitance of the load zone is not sufficient to fully describe the rolling bearing; the areas outside of the load zone must also be considered. This additional capacitance was investigated by Gemeinder et al. for point contact in ball bearings and by Schneider et al. for line contact in cylindrical roller bearings, both using a correction factor. The capacitance in the Hertzian zone is set in relation to the capacitance of the entire bearing by this correction factor. Particularly in operating regimes with low loads, the capacitance contribution from the areas outside the Hertzian contact area dominates, leading to models with correction factors becoming inaccurate [16,17]. The study and explicit calculation of the outside area in the raceway contact and the flange contact without the use of a correction factor are part of the present work. In addition to the capacitance model for the outside area, a model is developed to calculate the total capacitance of a cylindrical roller bearing, including both loaded and unloaded flanges.

1.2. Scope and Assumptions

In the present work, the model aims to determine the raceway capacitance using a model that relies on the operating parameters under radial load conditions. Additionally, it is possible to calculate the raceway capacitance using operating parameters both with and without axial load. The applied capacitance model does not incorporate any correction factors. Furthermore, the raceway capacitance is validated independently to ensure accuracy.

The following assumptions are made.

- There is an elastohydrodynamic lubrication (EHL) contact in the raceway contact.
- The shape of the contact area of each roller contact is the same as in the Hertzian case of dry contact [18].
- The flanges are flat and perpendicular to the raceways [19].
- A separating lubricating film forms at the point of flange contact, which can be described using an elastohydrodynamic lubrication model [19].
- The capacitance in the flange contact can be approximated by a parallel connection of infinitesimally small capacitors. Within these capacitors, the electrical-field lines are parallel to each other [5].
- The contact zones in the bearing are completely covered with lubricant [7].
- The surfaces are completely smooth; they have no roughness.
- The lubricant's permittivity ε_r is constant.

2. Materials and Methods

2.1. Bearing Geometry

When radial loads are transferred through a cylindrical roller bearing, a load-transferring contact is formed in the raceway contact. The size of the resulting contact area can be calculated according to Hertz's theory in line contact. The area of Hertzian contact is denoted by A_{Hertz}. If an axial load is applied to the bearing in addition to the radial load, a Hertzian point contact is formed at the flanges, depending on the lubrication conditions; see the red area in Figure 1 [20].

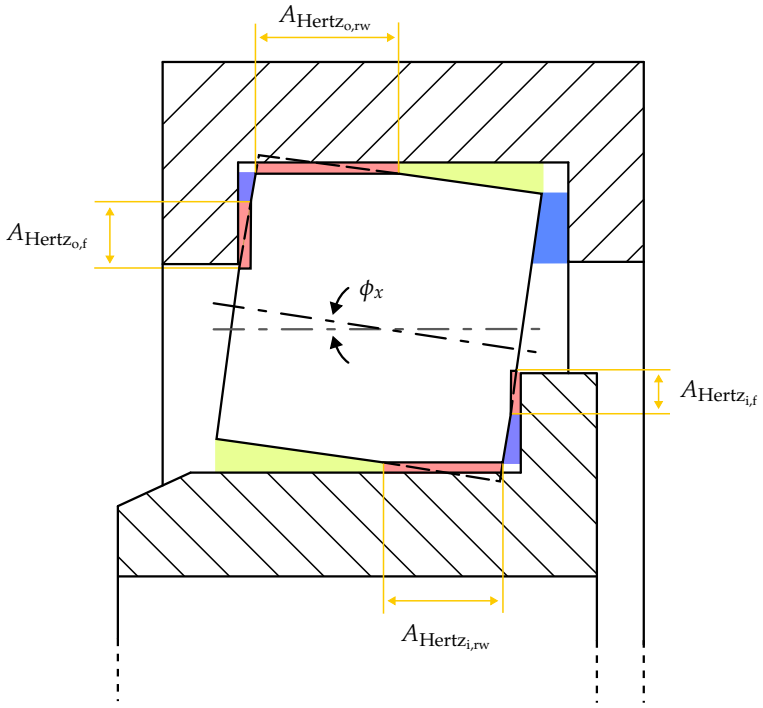


Figure 1. Overview of the areas in which different calculation methods are used; red: Hertzian area, yellow: outer area of the raceway contact; blue: outer area of the flange contact.

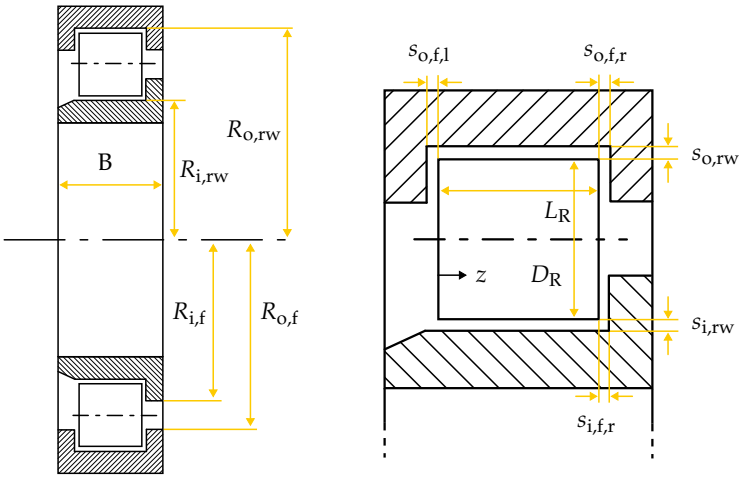
The area of a rolling element that is not part of the Hertzian area influences the capacitance of the bearing and must also be taken into account when calculating the bearing capacitance. In what follows, the area outside the Hertzian area is referred to as the "outside area"; see Figure 1, where yellow indicates the raceway surface contact and blue indicates the flange contact. The outside area extends both in the axial direction and in the circumferential direction of a rolling element.

To distinguish more clearly among the capacitance shares, a distinction is made between the capacitance of the inner ring and the rolling elements (denoted by the index *i*) and the capacitance between the outer ring and the rolling elements (denoted by the index *o*). Furthermore, a distinction is made between the capacitance of the raceway contacts and the capacitance at the flange contacts (denoted by *rw* and *f*, respectively). The flanges continue to be distinguished between the right side *r* and the left side *l*.

The loads acting on a rolling element or on the flanges must be calculated in order to determine the Hertzian areas. For this purpose, a simplified model according to Wang and Song is used [21].

The cylindrical roller bearing used in this work has a normal size of 208. All geometric dimensions are listed in Table 1 for an NJ-208 cylindrical roller bearing. The radii $R_{i,rw}$, $R_{o,rw}$, L_R and D_R are applied to all 208 cylindrical roller bearings regardless of the exact design. Depending on the specific bearing type (see Table 2), the number of flanges on the inner and outer rings varies.

Table 1. Geometry of the NJ-208 cylindrical roller bearing.

Section Plane 1	
B = 18 mm	
Inner Ring	**Outer Ring**
$R_{i,rw}$ = 24.75 mm $R_{i,f}$ = 27.25 mm	$R_{o,rw}$ = 35.75 mm $R_{o,f}$ = 34.15 mm
Section Plane 2	
Radial	**Axial**
$s_{i,rw} + s_{o,rw}$ = 25×10^{-3} mm–50×10^{-3} mm	$s_{i,f} + s_{o,f}$ = 23.5×10^{-3} mm–77.5×10^{-3} mm
$D_R = 2 \cdot R_R = L_R = 11$ mm	
Geometry	
	
Material Parameters	
Steel 100Cr6	**Ceramic Si3N4**
E_{Steel} = 207 GPa ν_{Steel} = 0.3 $\alpha_{t_{Steel}}$ = 11.15×10^{-6} K^{-1}	$E_{Ceramic}$ = 300 GPa $\nu_{Ceramic}$ = 0.26 $\alpha_{t_{Ceramic}}$ = 3.2×10^{-6} K^{-1}

All used bearings have a standard bearing clearance CN, from which the distances $s_{i,rw}$, $s_{i,f}$, $s_{o,rw}$ and $s_{o,f}$ are derived. In addition, bearings with ceramic rolling elements are

utilized for the tests conducted, as outlined in Table 2. The material properties for steel and ceramics shown in Table 1 are for this purpose.

The dimensions of the bearing, the elasticity moduli $E_{\text{Steel/Ceramic}}$, the transverse contraction coefficients $\nu_{\text{Steel/Ceramic}}$, and the thermal expansion coefficients $\alpha_{\text{Steel/Ceramic}}$ refer to a room temperature of 20 °C. The dimensions of the bearings are calculated at different temperatures using linear interpolation with the factor $\alpha_{\text{Steel/Ceramic}}$.

Considering that rolling elements of cylindrical roller bearings are not perfectly cylindrical and have a profile to reduce stress peaks at the edges, the rolling elements are divided into slices [22]. For each slice j, a specific diameter is calculated according to Equation (4) as a function of the axial coordinate z of the rolling element [23].

$$D_{\text{R}_\text{j}}(z_j) = 2 \cdot 0.00035 \cdot D_{\text{R}} \cdot \ln\left[\frac{1}{1-\left(\frac{2z_j}{L_{\text{R}}}\right)^2}\right] \tag{4}$$

The deflection δ_{e_j} of each slice is calculated using its diameter, considering that the deflection of one slice affects the deflection of the next slice of a rolling element. For this purpose, the slicing model developed by Sauer and Teutsch is used [22]. In the following model, each roller is divided into 100 slices to achieve a compromise between precision and computing time.

2.2. Raceway Capacitance Calculation

The total capacitance of the raceway can be represented by a capacitive component of the Hertzian area and a capacitive component outside the Hertzian area; see Figure 1. At this point, the focus is on the calculation of the capacitance outside the Hertzian area, as the calculation of the capacitance of the Hertzian area is calculated using the area A_{Hertz} and the central lubricating film thickness $h_{0,\text{line}}$ [17].

As Puchtler et al. have shown, the calculated capacitance is highly dependent on the direction of integration and whether the model is analytical or semi-analytical [5]. With regard to this, the calculation method for the capacitance in the outer area is divided into two cases. The application of each is determined by an individual decision for each slice of a roller, as uneven load distribution in the raceway contact at a contact point means that for some slices of a roller, the conditions for case 1 are met, while for other slices, the conditions from case 2 are met [24].

Case 1: The deflection δ_{e_j} of the EHL contact is less than the height of the lubricating film. The capacitance is calculated analytically; see Figure 2, left-hand side.

Case 2: The deflection δ_{e_j} of the EHL contact is greater than the height of the lubricating film. The capacitance is calculated semi-analytically; see Figure 2, right-hand side.

The analytic method used in case 1 is based on the concept from Puchtler et al. of equipotential lines between two electrically isolated eccentric electrodes. The charge carriers are the rolling element and the inner or outer ring; both are assumed to be perfectly smooth.

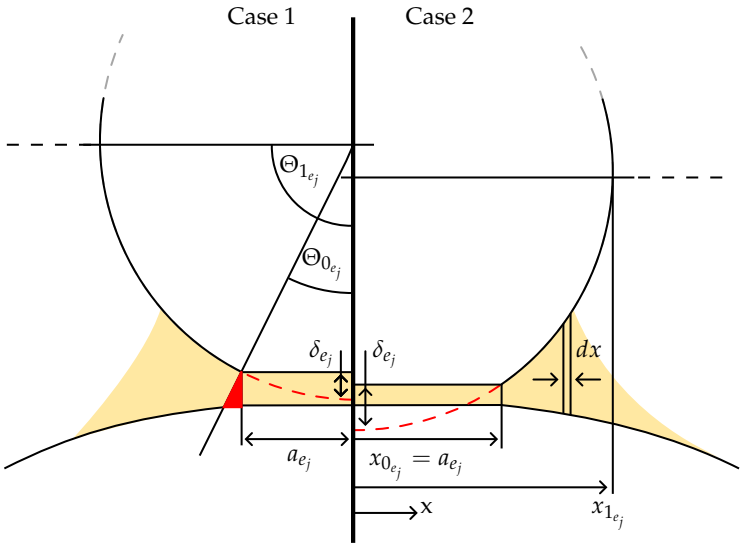


Figure 2. Left-hand side: Analytical model for calculating the capacitance of a rolling element slice outside the Hertzian surface with the limits of integration $\Theta_{0_{e_j}}$ and $\Theta_{1_{e_j}}$. Right-hand side: Semi-analytical model for calculating the capacitance of a rolling element slice outside the Hertzian surface with the integration limits $x_{0_{e_j}}$ and $x_{1_{e_j}}$.

On the boundaries of the electric field, the equipotential lines must coincide with the surface of these charge carriers. By varying the distance between the charge carriers, Apollonian circles meet these requirements and are used for the calculation below [5]. This calculation uses the auxiliary variable κ_{e_j} according to Equation (7). Furthermore, the variable τ_{e_j} is introduced according to Equation (5), representing the radius ratio between the raceway surface $R_{\mathrm{i/o,rw}}$ and the diameter of a slice of the rolling element D_{R_j}. Additionally, the dimensionless quantity α_{e_j} is introduced according to Equation (9), setting the distance between the outer surface of the rolling element and the raceway surface relative to the rolling element radius [24]. This quantity takes into account the rolling element's profiling, the deflection within the contact δ_{e_j}, and the lubricant film height $h_{0,\mathrm{line}}$. As outlined in Equation (11), the capacitance is calculated using these variables, in accordance with the boundary conditions detailed in Equation (10). The outer area commences at the termination of the Hertzian area, denoted by $\Theta_{0_{e_j}}$ and concludes at $\Theta_{1_{e_j}}$, as illustrated in Figure 2. To determine $\Theta_{0_{e_j}}$ the semi-axis a_{e_j} from the Hertzian area is used. This calculation method is applicable if the deflection in the rolling contact is less than the lubricating film thickness; otherwise, the equipotential lines touch. This condition is represented by Equation (8) [5]. Since the integration area of the analytical solution is mapped in cylindrical coordinates and the Hertzian surface is a plane, closer inspection reveals that part of the capacitance is neglected. The surface is shown in red in Figure 2 on the left [24].

$$\tau_{e_j} = \frac{2 \cdot R_{\mathrm{i/o,rw}}}{D_{\mathrm{R}_j}} \tag{5}$$

$$\sigma_{e_j} = \tau_{e_j} - 1 - \alpha_{e_j} \tag{6}$$

$$\kappa_{e_j} = \frac{1}{2 \cdot \sigma_{e_j}} \cdot \left(\tau_{e_j}^2 - \sigma_{e_j}^2 - 1 - \sqrt{\left(\tau_{e_j}^2 - \sigma_{e_j}^2 - 1 \right)^2 - 4 \cdot \sigma_{e_j}^2} \right) \tag{7}$$

$$\tau_{e_j} < \sigma_{e_j} + 1 \tag{8}$$

$$\alpha_{e_j} = \frac{-D_{\mathrm{R}_j} + D + 2 \cdot \left(-\delta_{e_j} + h_{0,\mathrm{line_e}}\right)}{D_{\mathrm{R}_j}} \tag{9}$$

$$\Theta_{0_{e_j}} = \arcsin\left(\frac{2 \cdot a_{e_j}}{D_{\mathrm{R}_j}}\right) \tag{10}$$

$$\Theta_{1_{e_j}} = \frac{\pi}{2}$$

$$C_{\mathrm{i/o,rw,anal_{e_j}}} = 4 \cdot \varepsilon \cdot \frac{\arctan\left[\frac{1+\kappa_{e_j}}{1-\kappa_{e_j}} \cdot \tan\frac{\Theta_{1_{e_j}}}{2}\right]}{\ln\left|\frac{\tau_{e_j}-\sigma_{e_j}-\kappa_{e_j}}{(\tau_{e_j}-\sigma_{e_j})\cdot\kappa_{e_j}-1}\right|} - 4 \cdot \varepsilon \cdot \frac{\arctan\left[\frac{1+\kappa_{e_j}}{1-\kappa_{e_j}} \cdot \tan\frac{\Theta_{0_{e_j}}}{2}\right]}{\ln\left|\frac{\tau_{e_j}-\sigma_{e_j}-\kappa_{e_j}}{(\tau_{e_j}-\sigma_{e_j})\cdot\kappa_{e_j}-1}\right|} \tag{11}$$

If the condition according to Equation (8) is not satisfied, Equation (7) can only be resolved in the complex number field, and the model is not applicable. For this reason, the integration is performed semi-analytically; see Figure 2, right-hand side. For this purpose, the integral shown in Equation (14) is calculated with the dimensionless boundary conditions $x_{0_{e_j}}$ and $x_{1_{e_j}}$; see Equation (13). The model divides the outer area into infinitesimal plate capacitors, which are connected in parallel, with the infinitesimal area $dA = dxdy$ and the infinitesimal height $h_{\mathrm{i/o},||_{e_j}}(x)$. Within these infinitesimal capacitors, it is assumed that the electric field lines run parallel. The distance between the rolling element and the raceway surface is calculated using Equation (12) [5]. A range of the height $h_{\mathrm{i/o},||_{e_j}}(x)$ cannot generally be determined, as it depends on the bearing size and the load conditions.

$$h_{\mathrm{i/o},||_{e_j}}(x) = \sqrt{\tau_{e_j}^2 - x^2} \cdot \mathrm{sgn}(\tau_{e_j}) - \sigma_{e_j} - \sqrt{1 - x^2} \tag{12}$$

$$x_{0_{e_j}} = \frac{2 \cdot a_{e_j}}{D_{\mathrm{R}_j}} \tag{13}$$

$$x_{1_{e_j}} = 1$$

$$C_{\mathrm{i/o,rw},||_{e_j}} = 2 \cdot \varepsilon \int_{x_{0_{e_j}}}^{x_{1_{e_j}}} \frac{1}{h_{\mathrm{i/o},||_{e_j}}} \, dx \tag{14}$$

2.3. Flange Capacitance Calculation

The calculation considered serves to determine the flange capacitance. First, the calculation of the area is explained, followed by the determination of the height $h(x)$. The area considered below is the intersection in the xy plane, consisting of the front surface of the rolling element cylinder and the ring surface of the flange; see Figure 3, left-hand side. To determine the area $A_{\mathrm{red}} + A_{\mathrm{green}}$, the upper halves of the red and green areas in the left-hand figure are calculated separately and then doubled. The red and green areas are then added together. The calculation is performed for the contact at the outer ring flange in the same way as for the contact at the inner ring flange; only the geometric parameters are changed. To do this, the angles β and γ of the red and green pitch circles are determined according to Equations (17) and (18). The angles are then used to determine the red and green pitch circles $\beta \cdot R_{\mathrm{R}}^2$ and $\gamma \cdot R_{\mathrm{f}}^2$.

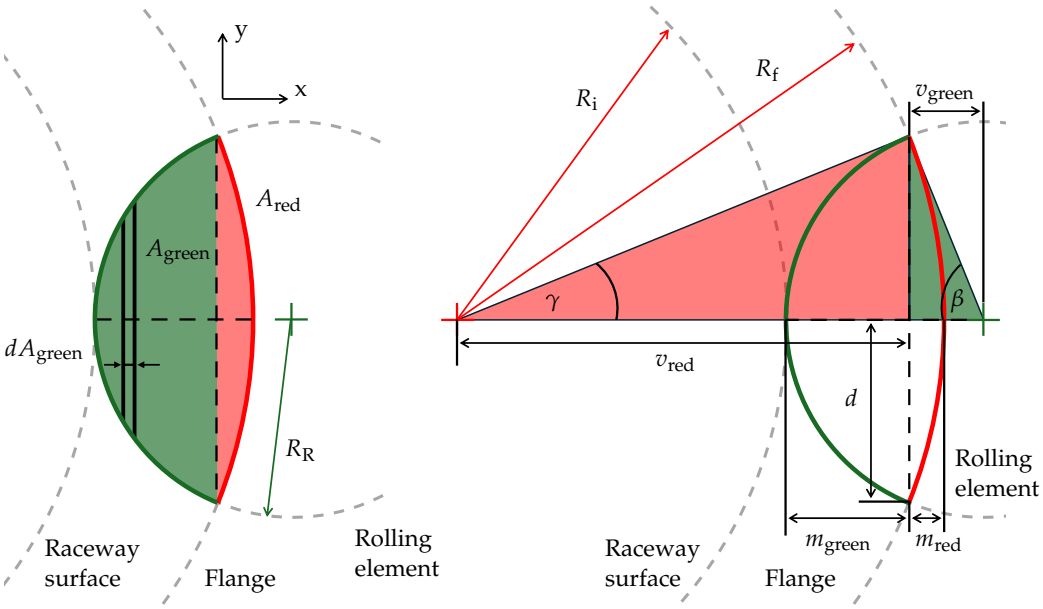


Figure 3. Left-hand side: Area of interest contains overlapping parts of the roller and flange marked with red and green. **Right-hand side**: Geometrical distances needed to calculate the overlapping areas.

To determine the lengths $v_{green,red}$ and $m_{green,red}$ according to Equations (15) and (16), a relationship is established between the hypotenuse, the adjacent side, and the opposite side d of the red and green triangles, respectively; see Figure 3 on the right.

Finally, the red and green triangles shown on the right-hand side in Figure 3 are subtracted from the corresponding red and green partial circles. The resulting areas, A_{red} and A_{green}, are doubled and added together to determine the intersection of the rolling element area and the flange area.

$$v_{green} = \frac{R_R^2 - R_f^2 - d_m^2}{2d_m}; v_{red} = \frac{R_f^2 - R_R^2 - d_m^2}{2d_m} \tag{15}$$

$$m_{green} = R_f \cdot (1 - \cos\gamma); m_{red} = R_R \cdot (1 - \cos\beta) \tag{16}$$

$$\beta = \begin{cases} \arccos\left(\frac{v_{green}}{R_R}\right) & \text{for } \gamma < \frac{\pi}{2} \\ \pi - \arccos\left(\frac{v_{green}}{R_R}\right) & \text{for } \gamma \geq \frac{\pi}{2} \end{cases} \tag{17}$$

$$\gamma = \arccos\left(\frac{v_{red}}{R_f}\right) \tag{18}$$

The height $h(x)$ is calculated according to Equation (19) from the constant component $h_{0,point}$ or δ_f and a component h_{tilt} that depends on x and ϕ_x, as shown in Figure 4. If a supporting lubricating film is present on the flange, the constant component is given by the height of the lubricating film, $h_{0,point}$. In the absence of a lubricating film, the constant component is determined by the half-axial bearing clearance $\frac{\delta_f}{2}$.

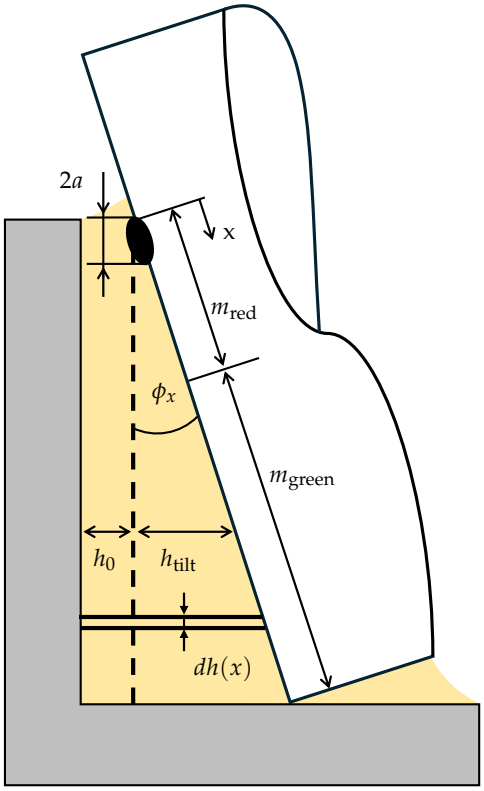


Figure 4. Schematic composition of the distance $h(x)$ which is dependent on the constant distance h_0 and the distance h_{tilt} dependent on the tilt angle ϕ_x.

The axial clearance of the bearing is calculated using the mean of the lower and upper limit dimensions. This makes the model independent of the specific bearing, meaning that measurement of the actual tolerance is unnecessary.

$$\begin{aligned} h(x) &= h_{0,\text{point}} + \sin(\phi_x) \cdot x \\ h(x) &= \frac{\delta_\text{f}}{2} + \sin(\phi_x) \cdot x \end{aligned} \tag{19}$$

The distance between the flange and the end face of the rolling element is not constant but varies with x. Therefore, calculating the total cross-sectional area and dividing it by the distance is an oversimplification. However, an infinitesimal piece dA of the area $A_{\text{red,green}}$ in the y-direction has the same distance between the flange and the end face. For this reason, the procedure described is not used in the model and is only introduced for clarity. In the model, the integral of the infinitesimal areas $dA_{\text{red,green}}$ is used to calculate the capacitance according to Equations (21) and (20) in the Cartesian coordinate system.

$$C_{\text{o,f,r}/l_e} = C_{\text{green}}(x,y) = 2 \cdot \varepsilon \int_{m_{\text{red,o}}}^{R_R} \int_{0}^{\sqrt{R_R^2+x^2}} \frac{1}{h(x)}\, dy\, dx \tag{20}$$

$$\begin{aligned} C_{\mathrm{i,f,r/l}_e} &= C_{\mathrm{red}}(x,y) + C_{\mathrm{green}}(x,y) \\ &= 2 \cdot \varepsilon \int_0^{m_{\mathrm{red}}} \int_0^{\sqrt{R_\mathrm{f}^2+x^2}} \frac{1}{h(x)}\, dy\, dx \\ &+ 2 \cdot \varepsilon \int_{v_{\mathrm{green}}}^{R_\mathrm{R}} \int_0^{\sqrt{R_\mathrm{R}^2-x^2}} \frac{1}{h(x)}\, dy\, dx \end{aligned} \tag{21}$$

2.4. Bearing Capacitance

In order to calculate the capacitance of the entire bearing, it is first necessary to define the bearing type and the bearing size, given that the calculation of the capacitance depends on the bearing type. To illustrate this point, it should be noted that bearings of the NU series have flanges exclusively on the outer ring. Conversely, bearings of the NJ series have one flange on the inner and two on the outer ring, while bearings of the NUP series are characterized by the presence of two flanges on the inner and outer rings. The number of flanges must be considered when determining the roller capacitance, as outlined in Equation (23).

$$C_\mathrm{B} = \sum_{e=1}^{Z} C_{\mathrm{R}_e} \tag{22}$$

The bearing capacitance C_B is calculated according to Equation (22) from the parallel connection of the capacitance of each individual roller C_{R_e}, whereby the bearing has a total of Z rollers. The capacitance of each roller is calculated from the capacitance share of the raceway contact on the inner ring $C_{\mathrm{i,rw}}$, the capacitance share of the raceway contact of the outer ring $C_{\mathrm{o,rw}}$, and the flange shares, which depend on the bearing type. The capacitance in the raceway surfaces $C_{\mathrm{i/o,rw}_e}$ consists of the sum of the partial capacities $C_{\mathrm{i/o,rw}_{e_j}}$ of the N slices of each roller.

$$\begin{aligned} C_{\mathrm{R}_e} &= \left[\frac{1}{C_{\mathrm{i}_e}} + \frac{1}{C_{\mathrm{o}_e}}\right]^{-1} \\ &= \left[\frac{1}{\sum_{j=1}^{N} C_{\mathrm{i,rw}_{e_j}} + C_{\mathrm{i,f,r}_e}} + \frac{1}{\sum_{j=1}^{N} C_{\mathrm{o,rw}_{e_j}} + C_{\mathrm{o,f,l}_e} + C_{\mathrm{o,f,r}_e}}\right]^{-1} \end{aligned} \tag{23}$$

Equation (23) shows an example of the equation used to calculate the capacitance of a rolling element within an NJ bearing. For this purpose, the capacitances at the inner-ring contact $C_{\mathrm{i,f,r}_e}$ and $\sum_{j=1}^{N} C_{\mathrm{i,rw}_{e_j}}$ are connected in parallel. The capacitances at the outer-ring contact $C_{\mathrm{o,f,l}_e}$, $C_{\mathrm{o,f,r}_e}$, and $\sum_{j=1}^{N} C_{\mathrm{o,rw}_{e_j}}$ are also connected in parallel. The resulting capacitances at the inner-ring contact C_{i_e} and at the outer-ring contact C_{o_e} are connected in series. An overview of the equivalent capacitances is shown in Figure 5. Since an NU bearing has no flange on the inner ring, Equation (23) must be adjusted by removing $C_{\mathrm{i,f,r}_e}$. The model is therefore modular and adaptable depending on the bearing type and can be applied equally to all cylindrical roller bearing types.

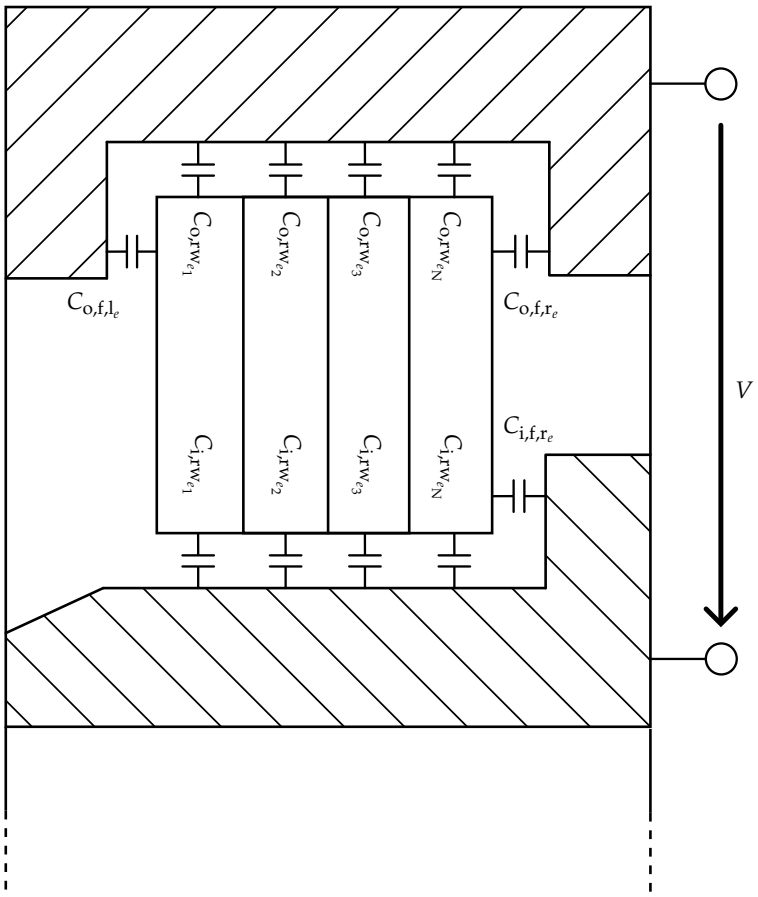


Figure 5. Electrical equivalent circuit diagram of a rolling element of an NJ bearing and integrated slice model.

2.5. Experimental Setup

The test bench and measuring device utilized by Puchtler et al. were used to measure the capacitance of the cylindrical roller bearings [6,25]. As these tests do not use radial deep groove ball bearings, bearings from the NUP series were installed in the test bench alongside the actual test bearing to ensure the shaft was clearly supported. In contrast to those used by Puchtler et al., the support bearings used in this study were not hybrid bearings.

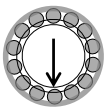
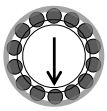
The test bench was set to different operating conditions during the tests; see Table 2. The individual test points were selected in random order so that any influence from previous tests could be ruled out.

The test points shown in Table 2 were examined on each bearing type. To ensure statistical reliability, the tests were performed three times with each bearing type. In order to guarantee a sufficient lubricating film, an oil flow rate of 10 L min^{-1} was selected with the reference oil FVA IIIa. A detailed description of the reference oil is available in Table 2. In addition, the lubricant viscosity was calculated according to the model of Vogel [26] and the pressure–viscosity coefficient was calculated according to a model developed by FVA [27]. The bearings used had an insulating cage made of glass-fiber-reinforced PA66.

The selected bearings differed in terms of the number of flanges and the materials used for the rollers. Modified bearings were used to measure the raceway capacitance. As these bearings do not have steel flanges but use plastic flanges to guide the rolling elements, only the capacitance of the raceway surfaces was measured [24]. In this work, these modified bearings are denoted as N0 bearings. Furthermore, NU bearings were used, which only have flanges on the outer ring. This quantifies the influence of the unloaded flanges on the capacitance. To measure the capacitance under axial load, bearings from the NJ series were

used and loaded with a load angle of up to 20°. The load angle describes the relationship between the axial and the radial load $\iota = \arctan F_a / F_r$ [28]. For the bearings used, a load angle of 20° is just below the static load limit for the given forces. Therefore, an increase in the axial load is not possible.

Table 2. Bearing type and experimental parameters.

Denotation	Icon	Denotation	Icon
N0-208		N0-208-Ceramic	
NU-208		NU-208-Ceramic	
NJ-208		NJ-208-Ceramic	

Experimental Parameter		Value
Radial load	F_r	1575 N, 2520 N, 3938 N, 6300 N, 10000 N, 15750 N
Load angle	ι	0°, 10°, 20°
Temperature	T_{Oil}	30 °C, 60 °C, 90 °C
Rotation speed	n	1000 min^{-1}, 3000 min^{-1}, 5000 min^{-1}, (7000 min^{-1})
Voltage frequency	f	4 kHz, 20 kHz, 100 kHz
Lubricant Parameter		**Value**
Density at 15 °C	ρ	878 kg m^{-3}
Viscosity at 40 °C	$\nu_k(40)$	92 mm s^{-1}
Viscosity at 100 °C	$\nu_k(100)$	10.6 mm s^{-1}
Relative permittivity	ε_r	2.2

To ensure that the support bearings did not affect the measurement results, open measurements were performed for each operating point using a bearing that had only ceramic rolling elements to measure the electric influence of the test bench, the measurement setup, the bearing seats, and the support bearings. This measured capacitance was subtracted from the measured value in the evaluation of the measurements, so the resulting capacitance depended only on the bearing capacitance.

During the tests, it became apparent that it was not possible to operate NJ bearings at a speed of 7000 min^{-1}, as the vibrations and temperature increased too much. It was also not possible to operate the NJ bearings under the conditions of 90 °C, 5000 min^{-1}, radial load of 15750 N and load angles of 0°, 10° and 20°, as too much heat was generated in these cases, and the bearing temperature rose above 140 °C, while the maximum temperature for PA66 cages was 120 °C.

2.6. Applied Hydrodynamic Lubrication Theory

Dowson and Toyoda used a lubricant model to calculate the lubricating film thickness, which depends on the parameters U, G and W. The limits of the model are defined by the ranges of these parameters investigated by Dowson and Toyoda. The model can be applied

as long as parameter U is between 10^{-9} and 10^{-13} and parameter W is between 2×10^{-4} and 6×10^{-5} [15].

The operating conditions set for the experiments (Table 2) result in the parameter W being outside the parameter range, as shown by Dowson and Toyoda at loads below 6300 N and at 15750 N. All of the rotational speeds used are within the parameter range of U. Errors in the lubricant model are known for the published ranges of values. For values outside these ranges, the model error is unknown. As the difference between the calculated and measured capacitances does not increase rapidly outside these ranges, which would therefore indicate a modeling error, load parameters outside the range published by Dowson and Toyoda are also presented. The lubricant model was corrected using the thermal correction factor of Zhou and Hoeprich, which considers the heating of the oil by the pressure within the pressing and shearing processes [29].

In Section 1.2, it is assumed that the surfaces are smooth. The influence of surface roughness on the capacitance is considered to be negligible according to the literature, provided that the lubricating film is larger than the roughness peaks [18]. As this is only relevant in the transition to mixed friction and the present work considers only the EHL regime, the influence of surface roughness is considered negligible.

3. Results and Discussion

Due to the sequential setting of the operating parameters, the test bench control was sometimes not able to set the target temperature, resulting in deviations of more than 10 °C between the set and measured temperatures in some cases. To prevent this deviation in the operating parameters from leading to deviations between the measured capacitance and the calculation, the measured operating parameters of temperature, axial load, radial load, and speed were used as input parameters for the calculation. This reduced the influence of control deviations on the extent of measurement errors.

Axial loads of less than 500 N could not be applied during the tests. For this reason, operating points with axial loads of less than 500 N were not considered in the following analysis.

In elastohydrodynamic lubrication (EHL), the bearing predominantly has a capacitive behavior and is expected to result in a phase angle of $-90°$, which is also subject to slight fluctuations in reality. In the boundary friction regime, the bearing's predominant behavior is resistive, resulting in a phase angle of $0°$.

As there is partial metal-to-metal contact in mixed lubrication, the phase angle fluctuates noticeably but does not average at $-90°$. To determine operating points within the EHL regime that allow a certain phase angle fluctuation around $-90°$, a Gaussian mixture model was used. For each measurement, a probability was calculated to indicate the likelihood of the phase angle deviating from $-90°$ due to scattering rather than mixed friction. Data points with a probability greater than 95% could be reliably assigned to the EHL regime. Those with probabilities below 5% were reliably assigned to the mixed friction regime. Those with a probability between 5% and 95% were assumed to belong to the EHL regime, with the deviation from the theoretical phase angle of $-90°$ assumed to be due to scattering.

Increasing the confidence interval from 95% to 99% increased the reliability of assigning data points to the EHL and confirmed that EHL conditions were present in the data point; less scattering was accepted. However, this also resulted in many data points being assigned to mixed friction that actually lie within the EHL. To achieve a compromise between certainty and scattering, a confidence level of 95% was chosen.

When comparing the calculated probabilities of the measurements with the phase angles, it is noticeable that data points between −95° and −82° are assigned to the EHL regime. At high loads, and particularly at 90 °C, the EHL criterion is not always satisfied.

3.1. Raceway Capacitance

In order to evaluate the overall model, first, the sub-model that exclusively represents the raceway–surface capacitance was considered. For this purpose, the capacitance of the N0-208 bearings was measured. In these bearings, the steel flanges were replaced with plastic flanges so that they have a negligible influence on the capacitance. Figure 6 compares the calculated and measured capacitances at different temperatures and radial loads, at a speed of 5000 min^{-1}. Three different measurement frequencies and three bearings of the same type were used, resulting in nine measurements for each operating parameter. These are presented as mean values with their corresponding standard deviations. The calculation results are shown as dashed lines. As can be seen in Figure 6, the agreement between the measured value and the calculated result is quite good, even though there is increasing deviation with rising temperature.

3.2. Capacitance of Axial Unloaded Bearings

In addition to the raceway capacitance, the model must also consider the capacitance of the flange. To examine the quality of the flange-contact modeling, tests were carried out using NU-208 bearings with steel flanges on the outer ring only, which are unable to carry axial loads. A comparison of the measurement and calculation results is shown in Figure 7.

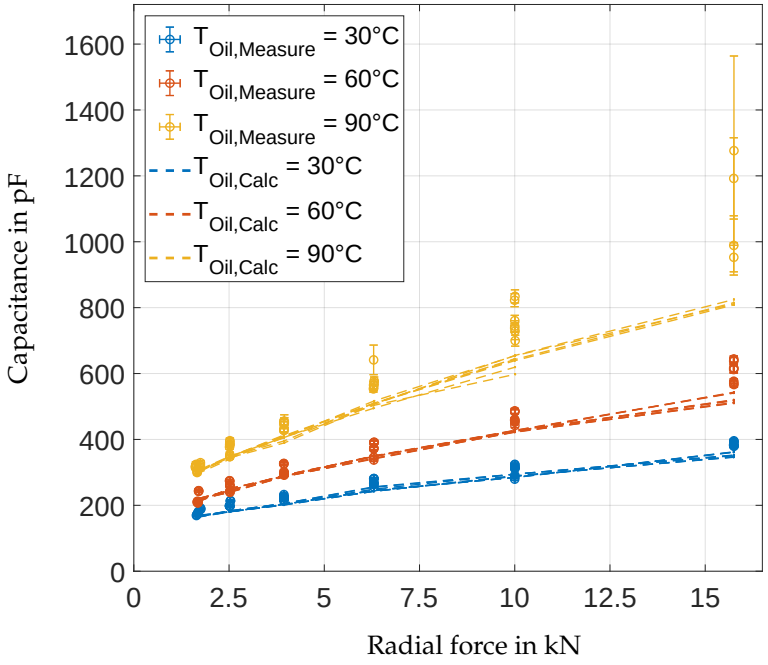


Figure 6. Measured and calculated capacitance of an N0-208 bearing as a function of radial force for different lubricant temperatures and rotational speed of 5000 min^{-1}.

Compared to Figure 6, the deviation between the calculation and the measurement in Figure 7 is more dependent on temperature, which is particularly evident at a temperature of 90 °C. For both 30 °C and 60 °C, the measurement and experiment averages deviate by 10%. For 90 °C, the deviation is 19%. This deviation is also evident when comparing the temperatures in Figure 7.

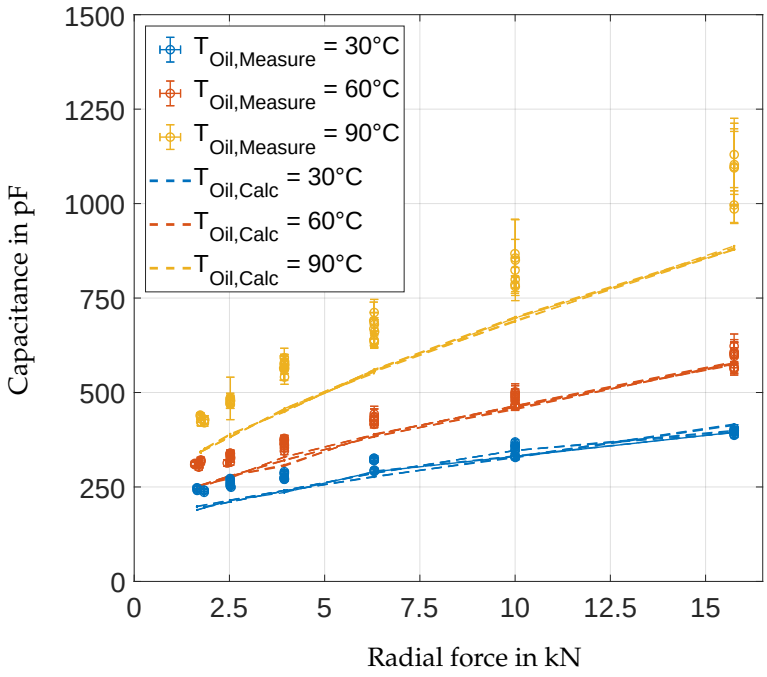


Figure 7. Measured and calculated capacitance of a NU-208 bearing as a function of radial force for different lubricant temperatures and rotational speed of 5000 min^{-1}.

Since the total bearing capacitance is a superposition of the raceway and flange capacitance (see Section 2.4) and the raceway contact agreement is greater (see Figure 6), it can be concluded that the model error originates from the flange capacitance model.

As the error increases with rising lubricant temperature and is derived from the flange model, it can be concluded that there is a temperature dependency in the flange model that has not been taken into account. The dominant factor influencing the flange capacitance is the distance between the rolling elements and the flange, which is calculated as an average value independent of temperature in the present model; see Section 2.3.

For a more detailed analysis of the capacitance shares, Figure 8 compares the measured capacitance with the calculated capacitance. Additionally, the capacitance shares resulting from Hertzian contact, the outer area of the raceway, and flange contact are presented. As the partial capacitances must be calculated in series with each other, it is not possible to add them together to calculate the total capacitance; see Section 2.4.

As shown in the figure, the capacitance of the flange is constant. As there is no force dependency of the capacitance on an unloaded flange, it depends exclusively on the constant axial tolerance. It is also evident that the capacitance of the outer area exceeds the capacitance of the Hertzian area by a nearly constant factor. This observation is consistent with the assumption made in other literature, where the capacitance in the outer area is represented by the capacitance of the Hertzian surface multiplied by a constant factor [16,17]. Similar to the capacitance from Hertzian contact, the capacitance of the outer area depends directly on the distance between the rolling element surface and the raceway surface. A greater load reduces the distance between the surfaces to the same extent, increasing the capacitance of both the Hertzian area and the outer area.

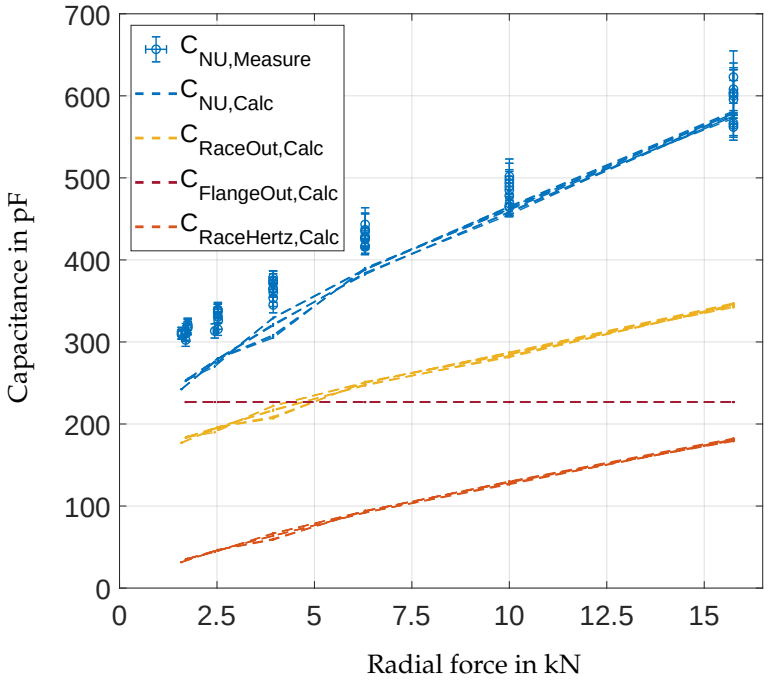


Figure 8. Measured and calculated capacitance of a NU-208 bearing as a function of radial force at 5000 min^{-1} and 60 °C. The calculated capacitance is divided into the individual components.

3.3. Capacitance of Axially Loaded Bearings

NJ-type cylindrical roller bearings can transmit axial loads via the flange on the inner ring. To evaluate the model in this case, the NJ bearings are subjected to axial loads. The results of the measurements and the corresponding calculation results are shown in Figure 9.

As this model is only applicable at EHL conditions and at 1000 min^{-1}, there exist many operating points in mixed friction. The presented operation points are at higher rotational speeds to increase the lubricant film thickness. Because 5000 min^{-1} generated too much heat, Figure 9 show the operating points at 3000 min^{-1} and not 5000 min^{-1} (Figures 6 and 7).

As the bearings in the test reached temperatures of over 140 °C at load angles of 10° and 20°, with radial loads of 15750 N and velocities of 3000 min^{-1} and 5000 min^{-1}, these operating points could not be investigated, keeping in mind the temperature limit of the cages is 120 °C.

These operation conditions are not present in the 60 °C and 90 °C tests at a load angle of 20°. The single data point at the specified load was generated by attempting to approach the operating point.

A significant increase in the overall capacitance of the bearing is evident when comparing Figures 7 and 9. This increase is due to the axial load. At 60 °C and 6300 N, the capacitance of the NU-208 bearing is approximately 400 pF. The NJ-208 bearing has a capacitance of 700 pF at the same operating point with a load angle of 10° and a capacitance of approximately 1150 pF at a load angle of 20°.

It is also evident that the nine single measurement results vary considerably more from each other at any given load–temperature combination, as shown in Figures 6 and 7. As this variation is not due to mixed friction, it must be caused by differences in the axial positioning of the inner ring and the rolling elements at the same operating point, which is not considered in the model.

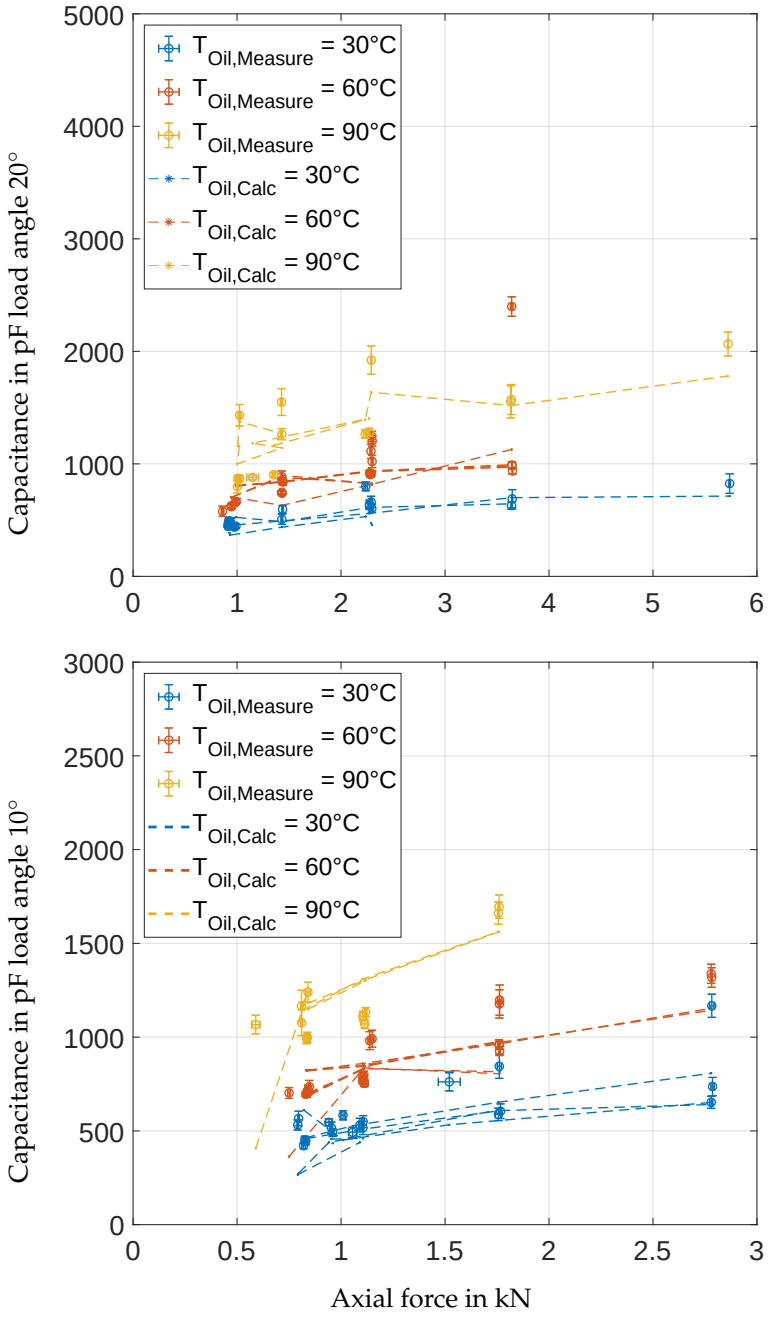


Figure 9. Measured and calculated capacitance of a NJ-208 bearing as a function of axial force for different lubricant temperatures, rotational speed of 3000 min^{-1}, and load angles 10° and 20°.

3.4. Overview of All Measured Values

To provide a comprehensive evaluation of the model, relative residuals related to the measured values were calculated. The rotation speeds were divided into the corresponding temperatures for this purpose and plotted against the radial force, divided by the bearing types. As the individual measurement frequencies in the EHL range were similar, the mean residual value for each operating point was calculated and is shown in Figure 10. White fields have no measured value, either because the operation condition generated too much heat or because it is in the mixed lubrication regime.

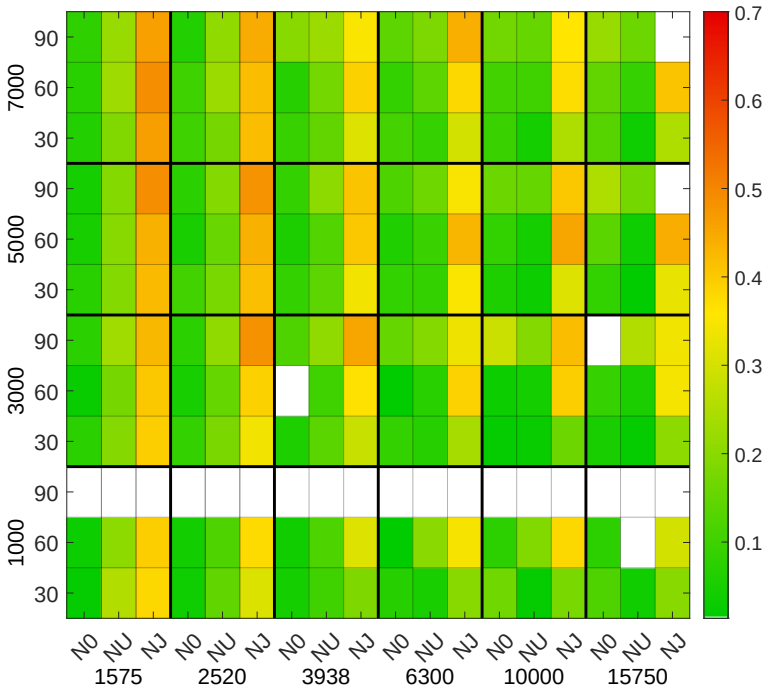


Figure 10. Average value of the relative residuals of an operating point broken down by rotation speed, temperature and radial load for N0-208, NU-208 and NJ-208 bearings. Axial loads are not taken into account.

As can be seen, the model shows good agreement for N0 and NU bearings with a relative residual of less than 20 % for a large proportion of the investigated operating points. The fact that Dowson and Toyoda did not investigate the lubricant model for small values of parameter W [15] does not appear to have a negative influence on the result of the lubricating film thickness calculation; see Section 2.6.

The relative error of NJ bearings is more noticeable than the error of the other bearing types. This is due to the unknown axial position of the inner ring without axial load, resulting in incorrect distances between the flange and the rolling element.

Looking at the residuals reveals that the error increases from the N0 to the NJ bearings, with the NU bearings being somewhere in between. This can be attributed to the complexity of the overall model. The NJ bearing capacitance model consists of the N0 sub-model and the individual flange-contact models, as detailed in Section 2.4. Each of these sub-models deviates from the actual value. These deviations are superimposed, resulting in a larger error for the more complex model. Therefore, the error in the NJ bearing calculation is the sum of various small deviations.

The measured values for the operating points that cannot be reached (see Section 2.5) originate from the first measurement series, during which it was determined that these operating points could not be set.

4. Conclusions

This paper presents a model for calculating the capacitance of cylindrical roller bearings. The model considers the following operating conditions: radial load, axial load, temperature, and rotational speed without using capacitance correction factors. By considering the raceway and flange contacts separately, the model accounts for the increase in capacitance caused by an axial load. This separation also makes the calculation method modular and applicable for different types of cylindrical roller bearings. As all calculation formulas depend on the bearing geometric parameters, the model is applicable to both different bearing types and different bearing sizes; see Sections 2.2 and 2.3.

The model was evaluated by measuring and comparing the capacitance for three different bearing types (N0-208, NU-208, and NJ-208) and under various operating conditions. At the test bench, the radial load, the axial load, the temperature, the rotational velocity, and the measurement frequency were varied. The bearing capacitance increases with increasing load, increasing speed, and increasing temperature. This behavior is captured by the present model. The discrepancy between measured and calculated capacitance varies in magnitude depending on the bearing type and operating conditions.

Additionally, the capacitance components resulting from the Hertzian area of a NU-208 bearing were compared with those of the outer region and those of the unloaded flanges, as shown in Section 3.2. Especially in the tests with axial load, many operating points either cannot be reliably set on the test bench or are in the mixed friction regime, which is outside the scope of this study. The operating points, classified within the EHL range, were determined using a Gaussian mixture model; see Section 3.

Compared to other models in the literature, which account for the capacitance in the outer area using a correction factor, the present model offers an approach to calculating the capacitance on the basis of physical relationships and provides an understanding of the electrical mechanisms in the rolling contact. The relationship between the capacitance resulting from the Hertzian area and the capacitance of the outside area, as used in the literature [16,17], is also recognized in this work; see Section 3.2.

Author Contributions: Conceptualization, J.M. and S.P.; methodology, J.M. and S.P.; software, J.M. and S.P.; validation, J.M. and S.P.; formal analysis, J.M. and S.P.; investigation, J.M. and S.P.; resources, J.M., S.P. and E.K.; data curation, J.M. and S.P.; writing—original draft preparation, J.M.; writing—review and editing, J.M., S.P. and E.K.; visualization, J.M.; supervision, S.P. and E.K.; project administration, J.M., S.P. and E.K.; funding acquisition, E.K. All authors have read and agreed to the published version of the manuscript.

Funding: This research was funded by the Deutsche Forschungsgemeinschaft (DFG, German Research Foundation)—556577310.

Data Availability Statement: The raw data supporting the conclusions of this article will be made available by the authors on request.

Conflicts of Interest: The authors declare no conflicts of interest.

References

1. He, F.; Xie, G.; Luo, J. Electrical bearing failures in electric vehicles. *Friction* **2020**, *8*, 4–28. [CrossRef]
2. Busse, D.; Erdman, J.; Kerkman, R.; Schlegel, D.; Skibinski, G. Bearing Currents and Their Relationship to PWM Drives. *IEEE Trans. Power Electron.* **1997**, *12*, 243–252. [CrossRef]
3. Muetze, A.; Strangas, E. The Useful Life of Inverter-Based Drive Bearings: Methods and Research Directions from Localized Maintenace to Prognosis. *IEEE Ind. Appl. Mag.* **2016**, *22*, 63–73. [CrossRef]
4. Graf, S.; Sauer, B. Surface Mutation of the Bearing Raceway During Electrical Current Passage in Mixed Friction Operation. *Bear. World J.* **2020**, *5*, 137–147.
5. Puchtler, S.; Schirra, T.; Kirchner, E.; Späck-Leigsnering, Y.; de Gersem, H. Capacitance calculation of unloaded rolling elements—Comparison of analytical and numerical methods. *Tribol. Int.* **2022**, *176*, 107882. [CrossRef]
6. Puchtler, S.; van der Kuip, J.; Kirchner, E. Analyzing Ball Bearing Capacitance Using Single Steel Ball Bearings. *Tribol. Lett.* **2023**, *71*, 38. [CrossRef]
7. Magdun, O.; Binder, A. Calculation of roller and ball bearing capacitances and prediction of EDM currents. In *2009 35th Annual Conference of IEEE Industrial Electronics*; IEEE: New York, NY, USA, 2009; pp. 1051–1056. [CrossRef]
8. Manjunath, M.; Hausner, S.; Heine, A.; Baets, P.; Fauconnier, D. Electrical Impedance Spectroscopy for Precise Film Thickness Assessment in Line Contacts. *Lubricants* **2024**, *12*, 51. [CrossRef]
9. Maruyama T.; Radzi F.; Sato T.; Iwase S.; Maeda M.; Nakano, K. Lubrication Condition Monitoring in EHD Line Contacts of Thrust Needle Roller Bearing Using the Electrical Impedance Method. *Lubricants* **2023**, *11*, 223. [CrossRef]

10. Bader, N.; Furtmann A..; Tischmacher, H.; Poll, G. (Eds.) *Capacitances and Lubricant Film Thickness of Grease and Oil Lubricated Bearings: Rolling Element Bearings II: Rolling Element Bearing Dynamics*; VDMA Verlag: Frankfurt, Germany, 2017.
11. Coy, J.J. *Correlation of Asperity Contact-Time Fraction with Elastohydrodynamic Film Thickness in a 20-Millimeter-Bore Ball Bearing*. NASA Technical Publication; National Aeronautics and Space Administration: Washington, DC, USA, 1979; Volume 79.
12. Maruyama, T.; Maeda, M.; Nakano, K. Lubrication Condition Monitoring of Practical Ball Bearings by Electrical Impedance Method. *Tribol. Online* **2019**, *14*, 327–338. [CrossRef]
13. Schirra, T.; Martin, G.; Vogel, S.; Kirchner, E. Ball bearings as sensors for systematical combination of load and failure monitoring. In *DS 92: Proceedings of the DESIGN 2018 15th International Design Conference*; Design Conference Proceedings; Faculty of Mechanical Engineering and Naval Architecture, University of Zagreb, Croatia and the Design Society: Glasgow, UK, 2018; pp. 3011–3022. [CrossRef]
14. Hamrock, J.B.; Dowson, D. *Isothermal Elastohydrodynamic Lubrication of Point Contacts: III—Fully Flooded Results*; NASA Technical note; NASA: Boston, MA, USA, 1976.
15. Dowson, D.; Toyoda, S. A central film thickness formula for elastohydrodynamic line contacs. In *5th Leeds-Lyon Symposium on Tribology* ; Elsevier: Amsterdam, The Netherlands, 1978; pp. 60–65.
16. Gemeinder, Y.; Schuster, M.; Radnai, B.; Sauer, B.; Binder, A. Calculation and validation of a bearing impedance model for ball bearings and the influence on EDM-currents. In *2014 International Conference on Electrical Machines (ICEM)*; IEEE: New York, NY, USA, 2014; pp. 1804–1810. [CrossRef]
17. Schneider, V. The Electrical Modelling of Machine Elements. Ph.D. Thesis , Gottfried Wilhelm Leibniz Universität Hannover, Hannover, Germany, 2025.
18. NaNapel, W.; Bosma, R. The Influence of Surface Roughness on the Capacitive Measurement of Film Thickness in Elastohydrodynamic Contacts. *Proc. Inst. Mech. Eng.* **1970**, *185*, 635–639. [CrossRef]
19. Korrenn, H. The Axial Load-Carrying Capacity of Radial Cylindrical Roller Bearings. *J. Lubr. Technol.* **1970**, *92*, 129–134. [CrossRef]
20. Aramaki, H.; Cheng, H.S.; Zhu, D. Film Thickness, Friction, and Scuffing Failure of Rib/Roller End Contacts in Cylindrical Roller Bearings. *J. Tribol.* **1992**, *114*, 311–316. [CrossRef]
21. Wang, Z.; Song, J.; Li, X.; Yu, Q. Modeling and Dynamic Analysis of Cylindrical Roller Bearings Under Combined Radial and Axial Loads. *J. Tribol.* **2022**, *144*, 121203. [CrossRef]
22. Sauer, B.; Teutsch, R. An Alternative Slicing Technique to Consider Pressure Concentrations in Non-Hertzian Line Contacts. *Trans. ASME* **2004**, *126*, 436–442. [CrossRef]
23. *DIN 26281:2010-11*; Wälzlager–Dynamische Tragzahlen und nominelle Lebensdauer—Berechnung der modifizierten nominellen Referenz-Lebensdauer fuer Waelzlager. DIN Media GmbH: Berlin, Germany, 2010.
24. Ott, F. Elektrische Modellierung des Zylinderrolle-Laufbahn-Kontakts. Bachelor's Thesis, Universitäts- und Landesbibliothek Darmstadt, Darmstadt, Germany, 2024. [CrossRef]
25. Puchtler, S.; van der Kuip, J.; Becker-Dombrowsky, F.; Kirchner, E. Impedance measurement of rolling bearings using an unbalanced AC wheatstone bridge. *Front. Mech. Eng.* **2024**, *10*, 1456618. [CrossRef]
26. Vogel, H. Das Temperaturabhängigkeitsgesetz der Viskosität von Flüssigkeiten. *Phys. Z.* **1921**, *23*, 645–646.
27. Forschungsvereinigung Antriebstechnik e.V. *Schmierfilmdicke—Einfluss von Grundölart, Additivierung und Gebrauchszustand auf Viskositätsverhalten und Schmierfilmbildung*; FVA Abschlussbericht zum Forschungsvorhaben 400; RWTH Publications: Aachen, Germany, 2004.
28. Dahlke, H. *Handbuch Wälzlager-Technik: Bauarten, Gestaltung, Betrieb*; Springer Fachmedien: Wiesbaden, Germany, 1994.
29. Zhou, R.S.; Hoeprich, M.R. Torque of Tapered Roller Bearings. *J. Tribol.* **1991**, *113*, 590–597. [CrossRef]

Disclaimer/Publisher's Note: The statements, opinions and data contained in all publications are solely those of the individual author(s) and contributor(s) and not of MDPI and/or the editor(s). MDPI and/or the editor(s) disclaim responsibility for any injury to people or property resulting from any ideas, methods, instructions or products referred to in the content.